

Volatile organic compound fluxes over a winter wheat field by PTR-Qi-TOF-MS and eddy covariance

Benjamin Loubet^{1,*}, Pauline Buysse¹, Lais Gonzaga-Gomez¹, Florence Lafouge¹, Raluca Ciuraru¹, Céline Decuq¹, Julien Kammer^{1,a}, Sandy Bsaibes^{1,2}, Christophe Boissard^{2,3}, Brigitte Durand¹, Jean-Christophe Gueudet¹, Olivier Fanucci¹, Olivier Zurfluh¹, Letizia Abis^{1,b}, Nora Zannoni^{2,c}, François Truong², Dominique Baisnée², Roland-Sarda Esteve², Michael Staudt⁴ and Valérie Gros².

1 Université Paris-Saclay, UMR ECOSYS, INRAE, AgroParisTech, 78850, Thiverval-Grignon, France.

2 Laboratoire des Sciences du Climat et de l'Environnement, LSCE, UMR CNRS-CEA-UVSQ, IPSL, 91191 Gif-sur-Yvette, Île-de-France, France.

3 Université de Paris and UPEC, CNRS, LISA, F-94000 Créteil

4 Centre d'Ecologie Fonctionnelle et Evolutive UMR 5175, CNRS - Université de Montpellier - Université Paul-Valéry Montpellier – EPHE Campus CNRS, 1919 Route de Mende, F-34293 Montpellier cedex 5, France

a now at Department of Chemistry and Environmental Research Institute, University College Cork, T12 YN60 Cork, Ireland.

b now at Technische Universität Berlin, Umweltchemie und Lufttrinhaltunz, Straße des 17. Juni 135, Berlin, 10623, Germany.

c now at Max-Planck Institute for Chemistry, Hahn-Meitner-Weg 1, 55128 Mainz, Germany

* Corresponding author: Benjamin.Loubet@inrae.fr

1 Calibration factor of the PTR-QI-TOF-MS

Table S1. Adjustment of the PTR-QI-TOF-MS calibration factor with time. This adjustment was performed based on the 5 calibrations, the changes in E/N the 29/06/2016 and of the MCP detector before the 29/06. *S* is the calibration factor used in eq. (4) for all compounds except water vapour and methanol. For methanol *S* was multiplied by 2.66 based on a specific calibration performed for this compound. For water vapour *S* was computed hourly based using the infrared gas analyser.

Date	E/N	MCP	<i>S</i>	Std. Err.	R2
31/05/2016	150	2150	2.06	0.05	1.00
13/06/2016	150	2200	2.47	0.07	1.00
17/06/2016	150	2250	2.88	0.10	1.00
23/06/2016	150	2300	3.29	0.13	0.99
29/06/2016*	150	2300	3.29	0.13	0.99
29/06/2016 [#]	129	2300	3.49	0.12	1.00
01/07/2016	129	2300	3.45	0.12	1.00
07/07/2016	129	2300	3.28	0.11	0.99
21/07/2016	129	2300	2.89	0.11	0.99

2 VOC eddy-covariance fluxes computation

30 In this section, the development of equation (6) is explained in details. This equation was derived by considering two issues: (1) the fact that the PTR- Qi-TOF- MS is measuring mixing ratio in wet air and not dry air, and (2) the fact that the cps is normalised by the primary ion source when calculating the mixing ratio in eq. (1).

2.1 Accounting for the contribution of water vapour in eddy-covariance fluxes computation with the PTR-Qi-TOF-MS

35 Eq. (5), which is reproduced below for clarity sake, is based on $\chi_{i,d}$, the mixing ratio in dry air of compound i :

$$F_i = \frac{\overline{p_a^d}}{RT_a} \overline{w' \chi_{i,d}'} \quad (S1)$$

However, since the PTRMS measures a mixing ratio in wet air χ_i , its relation to $\chi_{i,d}$ needs to be accounted for:

$$\chi_{i,d} = \chi_i \times \frac{p_{drift}}{(p_{drift} - p_{v,drift})} \quad (S2)$$

Where $p_{v,drift}$ is the vapour pressure density in the drift. We also notice that:

$$40 \quad \frac{p_{drift}}{p_{drift} - p_{v,drift}} = (1 + \chi_{v,drift,d}) \quad (S3)$$

Where $\chi_{v,drift,d}$ is the water vapour mixing ratio in dry air in the drift. Considering eqns. (S2) and (S3), yields:

$$\chi_{i,d} = \chi_i \times (1 + \chi_{v,drift,d}) \quad (S4)$$

Which can be differentiated to give:

$$\chi'_{i,d} = \chi'_i \times (1 + \chi_{v,drift,d}) + \chi_i \cdot \chi'_{v,drift,d} \quad (S5)$$

45 When injecting eq. (S5) in eq. (S1), one then gets the following expression for the flux:

$$F_i = \frac{\overline{p_a^d}}{RT_a} \cdot \left[(1 + \overline{\chi_{v,drift,d}}) \cdot \overline{w' \chi'_i} + \overline{\chi_i} \cdot \overline{w' \chi'_{v,drift,d}} \right] \quad (S6)$$

Where $\overline{w' \chi'_{v,drift,d}}$ is the covariance of water vapour which can be expressed as a function of water vapour flux E ($\text{g m}^{-2} \text{s}^{-1}$):

$$w' \chi'_{v,drift,d} = \frac{E RT_a}{M_v p_a} \quad (S7)$$

50 where M_v is the water molar mass (g mol^{-1}). Assuming further that the drift water vapour pressure mixing ratio $\chi_{v,drift,d}$ is equal to the ambient one and equal to $\frac{p_{vap}}{p_a}$, one gets the following expression of the flux of compound χ_i :

$$F_i = \frac{\overline{p_a^d}}{RT_a} \cdot \left(1 + \frac{p_{vap}}{p_a} \right) \cdot \overline{w' \chi'_i} + \frac{\overline{p_a^d}}{RT_a} \cdot \overline{\chi_i} \cdot \frac{E RT_a}{M_v p_a} \quad (S8)$$

This hypothesis relies on the fact that the proportion of water vapour that is ionised is small, which is reasonable

55 since a small fraction of water vapour is ionised. Finally, we can factorise $\overline{w' \chi'_i} \times \frac{\overline{p_a^d}}{RT_a}$ in (S8) to yield the following expression:

$$F_i = \overline{w'\chi_i'} \times \frac{\overline{p_a^d}}{RT_a} \times \left(1 + \frac{p_{vap}}{p_a} + \frac{1}{V_{exch,i}} \cdot \frac{E}{M_v} \cdot \frac{RT_a}{p_a} \right) \quad (S9)$$

Where $V_{exch,i}$ (in m s^{-1}) is the exchange velocity of compound i and is equal to $\overline{w'\chi_i'}/\overline{\chi_i}$. In this equation, the term p_{vap}/p_a accounts for dilution due to water vapour and the term on the right-hand side of the parenthesis accounts for correlated fluctuations of the water vapour mixing ratios in the drift tube. In practice, the correction terms were evaluated using the QCL water vapour measurements that were made in the same sampling tube and allowed to evaluate E and p_{vap} . This correction term will only be large for compounds with small exchange velocities $V_{exch,i}$, hence with small interest in terms of ecosystem exchange. Indeed, if we want this term to remain smaller than ε , we find that $V_{exch,i}$ should be larger than $ERT_a/(M_v p_a \varepsilon)$. Taking the maximum evaporation condition which is typically $E \sim 0.2 \text{ g m}^{-2} \text{ s}^{-1}$, and taking a maximum affordable $\varepsilon = 0.25$ we find that $V_{exch,i} > 0.1 \text{ cm s}^{-1}$. For depositing compounds, this is a quite small deposition velocity. For emitting compounds, it depends on the atmospheric composition: compounds having large mixing ratios will lead to larger correction terms than those with low mixing ratios. On average, the correction term was found negligible over the campaign except for some compounds, which showed for a limited amount of time a correction larger than a few percent. These included noticeably acetone, for which the median correction was around 3%.

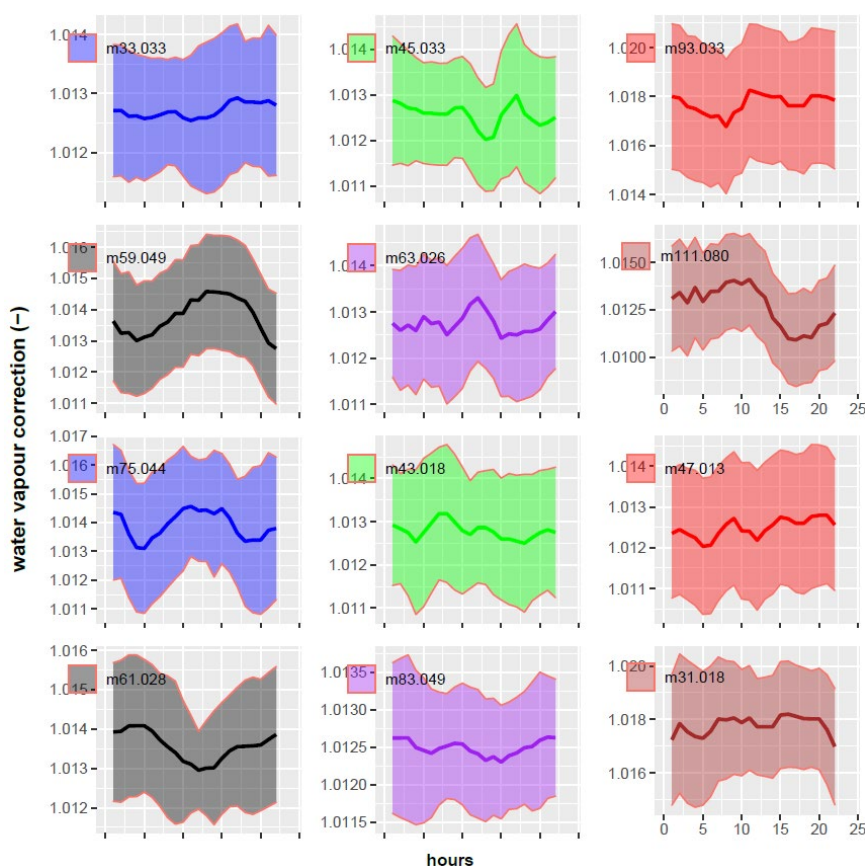


Figure S1. Example effect of water vapour dilution and fluctuations on the fluxes of the 6 most emitted and 6 most deposited VOCs.

2.2 Effect of ion source normalisation in eddy-covariance fluxes computation

An additional issue when using a PTRMS to measure fluxes by eddy-covariances, is the fact that the primary ion from the source (H_3O^+) is consumed by all compounds protonated and hence shows a fluctuation that is correlated with w . Usually in a PTRMS, the assumption is made that the consumption of H_3O^+ ions in the drift chamber is limited (lower than 10% of produced H_3O^+) which hence allows to assume pseudo first order chemical reaction rates (Holzinger et al., 2019). Although this assumption holds in most conditions, the issue is somewhat different when looking at fluctuations (and not mean quantities). In particular, in the mixing ratios computations (eq. 1 to 3), there is a “normalisation” step that involves dividing by $cps_{H_3O^+}^{trans} + cps_{H_2O.H_3O^+}^{trans}$. The question arises whether this normalisation should be done on the raw data prior to covariance calculation or on the computed covariances. To the best of our knowledge, this question has not been addressed before. To answer this question, we differentiate eqns. (1 - 4) and combine them with eq. (S9). In the differentiation process, we have considered all terms, except counts per seconds (cps), to be constant, which is justified by the assumption that they should not be correlated with w and will hence disappear when introduced in eq. (S9). We eventually find:

$$\chi'_i = S_i \times \chi_{i,ptr} \times \left\{ \frac{cps'_{R_iH^+}}{cps_{R_iH^+}} - \frac{\left(cps'_{H_3O^+} + \frac{TR_{H_3O^+}}{TR_{H_2O.H_3O^+}} cps'_{H_2O.H_3O^+} \right)}{(cps_{H_3O^+}^{trans} + cps_{H_2O.H_3O^+}^{trans})} \right\} \quad (S10)$$

Incorporating eq. (S10) into eq. (S9), simplifying the notation $cps_i = cps_{R_iH^+}$, and $tr_v = \frac{TR_{H_3O^+}}{TR_{H_2O.H_3O^+}}$, one gets:

$$F_i = S_i \left(\frac{\chi_{i,ptr}}{cps_i} \right) \left(\overline{w' cps'_i} - \frac{cps_i}{cps_{H_3O^+}^{trans} + cps_{H_2O.H_3O^+}^{trans}} \overline{w' (cps'_{H_3O^+} + tr_v cps'_{H_2O.H_3O^+})} \right) \times \frac{\overline{p_a^d}}{RT_a} \times \left(1 + \frac{p_{vap}}{p_a} + \frac{1}{v_{exch,i}} \cdot \frac{E}{M_v} \cdot \frac{RT_a}{p_a} \right) \quad (S11)$$

The normalisation factor here is $\overline{\chi_{i,ptr}}/cps_i$, which, based on eqns. (1) and (2) can be expressed as follows:

$$\overline{\chi_{i,ptr}}/cps_i = 1.657 e^{-11} \times \frac{U_{drift} T_{drift}^2}{k P_{drift}^2} \times \frac{TR_{H_3O^+}}{TR_{R_iH^+}} \left(\frac{1}{cps_{H_3O^+}^{trans} + cps_{H_2O.H_3O^+}^{trans}} \right) \quad (S12)$$

In practice, when computing the flux, if the covariance is calculated on non-normalised cps , the term including $cps'_{H_3O^+} + tr_v cps'_{H_2O.H_3O^+}$ in eq. (S11) is not taken into account and the normalisation is simply done with the normalisation factor in eq. (S12). If the cps are normalised prior to the covariance calculation, then an additional term in eq. (S11) appears that is mostly negative. Indeed, $cps'_{H_3O^+} \gg tr_v cps'_{H_2O.H_3O^+}$ and $\overline{w' cps'_{H_3O^+}}$ is usually negative because the sum of VOCs and water emissions are usually larger than deposition and hence $cps'_{H_3O^+}$ is inversely proportional to the sum of VOCs and water (it is consumed by reaction these compounds). This term can be rearranged to show up the biased and unbiased flux:

$$F_i^{biased} = F_i^{unbiased} (1 - A) \quad (S13)$$

Where:

$$A = \frac{cps_i}{cps_{H_3O^+}^{trans} + cps_{H_2O.H_3O^+}^{trans}} \frac{\overline{w' (cps'_{H_3O^+} + tr_v cps'_{H_2O.H_3O^+})}}{\overline{w' cps'_i}} \quad (S14)$$

In Figure S2 we have evaluated the magnitude of this additional term by comparing the fluxes calculated by normalising before and after covariance computation. We see that this has little effect on the methanol flux (less than a few %) except during some nights. This is explain by the fact that the covariance $\overline{w' cps'_{H_3O^+}}$ is multiplied by a factor that is inversely proportional to the ion source strength and is hence very small (lower than $3 \cdot 10^{-3}$). Hence, even if it is 10 times the compound flux, it remain small.

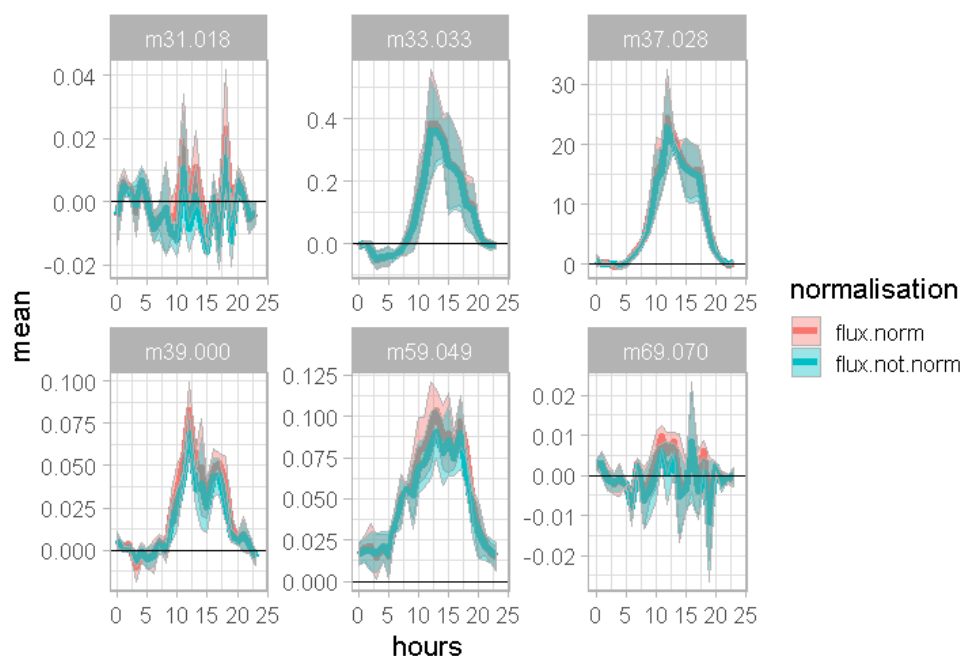


Figure S2. Example effect of cps normalisation on the fluxes of some key compounds. Red curves (flux.norm) correspond to flux calculated using normalised cps, while blue curves (flux.not.norm) correspond to fluxes calculated using raw cps.

In Figure S3, we show the term $(1 - A)$, which is the ratio of biased to unbiased flux, averaged over the whole period. It shows that the averaged bias is lower than 10% either positive (methanol, acetaldehyde) or negative (acetone). The bias is only large during the night and can vary between situations (interquartile up to 20%), but is most of the time lower than a few percents.

The main finding here is therefore that when normalisation is performed on a raw signal, an additional term should be taken into account but it seems to be in general quite small. On the contrary, if normalisation is performed after calculating the covariance on cps_i raw signals no additional term needs to be taken into account. In this study, we therefore chose to perform normalisation after covariance computation at a 5 min time step.

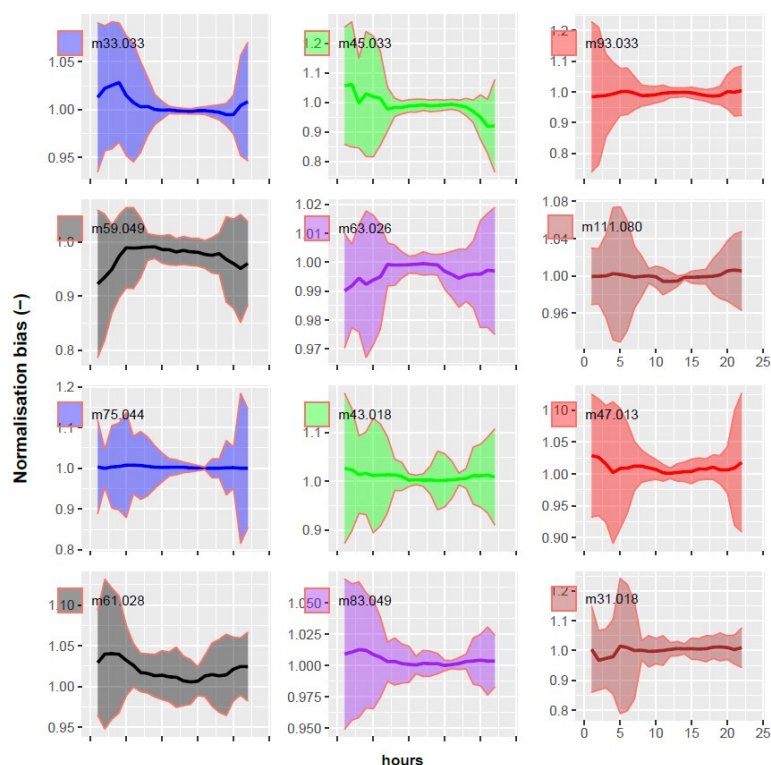


Figure S3. Bias introduced by normalising the cps by the primary ion prior to calculating the covariance, for the 6 most emitted and 6 most deposited compounds. Term (1-4) in equation (S13).

3 Lag decorrelation time and high frequency losses corrections

The decorrelation time lag was determined as the maximum of the correlation function between the vertical component of the wind speed and the component mixing ratio (or temperature). It can be seen from the example in **Figure S4** that the correlation functions for the instruments positioned at the end of the sampling line had a ~2.5 s delay and that the shapes of the correlation functions are very similar between air temperature (T_a) and mixing ratios from the QCL and the PTRMS. The PTRMS has a somewhat shorter lag time than the QCL, which can be explained by the smaller tube diameter and length between the main sampling line and the PTRMS subsampling, as well as the lower drift tube volume, compared to sampling system and optical cell of the QCL.

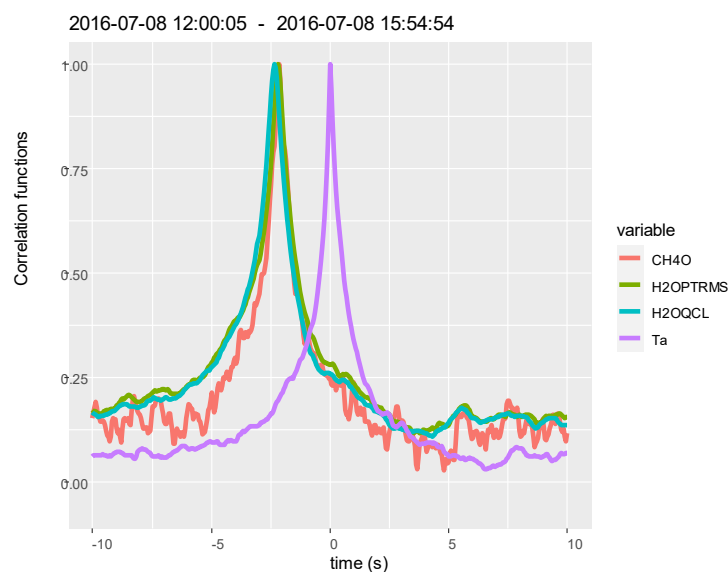


Figure S4. Example correlation functions between vertical component of the wind speed, sonic air temperature (T_a), the water vapour mixing ratio measured the QCL (H_2O_{QCL}) and the first H_2O cluster ion (H_2O_{PTRMS}). Data from 8 July from 12 to 16 hours UTC..

High frequency losses is an issue when measuring a flux using a long sampling line. The conditions chosen in this experiment ensured a short lag time as shown in **Figure S4**, suggesting high frequency losses should be small. Evaluation of these with the theoretical approach of Massman et al. (1991) provides an estimate of around 5% attenuation. However, in-situ measurements are more powerful for obtaining real conditions attenuations. The cross-spectra for the QCL water vapour and the PTRMS first water cluster were therefore computed and compared to the temperature cross-spectra (**Figure S5**). Water vapour proxy was used, since for other VOC, the cross-spectra was too noisy to compute a high frequency loss. We computed from co-ogives that high frequency losses represented less than a few percent of the flux for the water vapour cluster (Ammann et al., 2006). Usually, the QCL water vapour measurement showed higher HF losses than the first water cluster measured by the PTRMS, which is consistent with the slightly higher lag time observed in **Figure S4**.

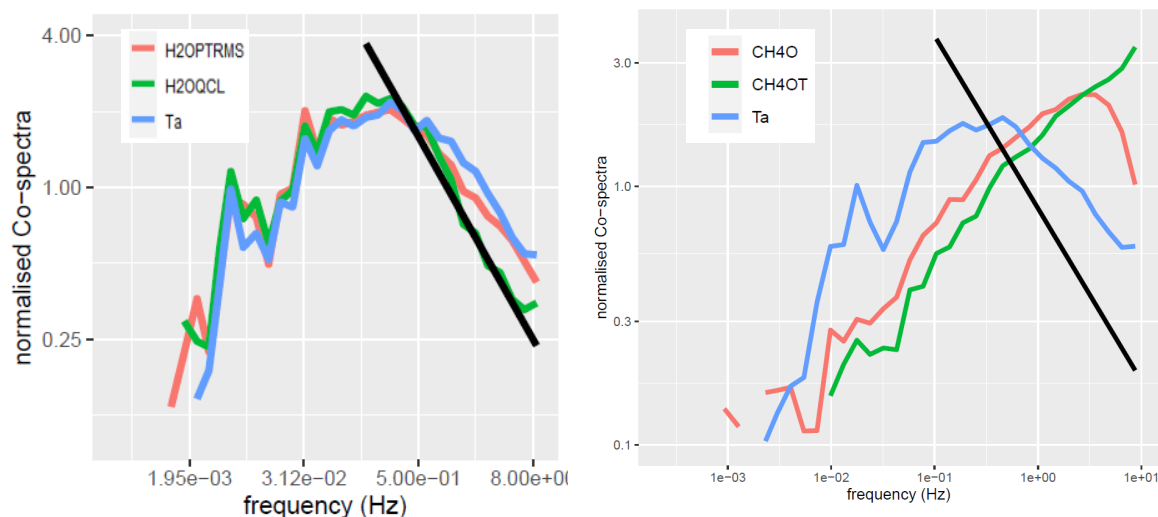


Figure S5. Normalised cross-spectra multiplied by the frequency. Shown are the cross spectrum between vertical component of the wind speed (W), sonic air temperature (Ta), the water vapour mixing ratio measured the QCL (H2OQCL), the first H₂O cluster ion (H2OPTRMS), the methanol (CH4O) and a mimic of the methanol signal based on the temperature signal plus noise (CH4OT). The cross spectra have been normalised by their mean values. Data from 8 July from 12 to 16 hours UTC. The black line shows the expected decrease in co-spectra for high frequencies based on the Monin Obukhov energy cascade theory ($\text{CoSP} \sim f^{3/2}$). The CH4OT signal was computed as the temperature signal centred and normalised by the variances of methanol to temperature on which was added a white noise of mean and standard deviation equal to that of methanol.

4 Water vapour mixing ratios and fluxes as measured by the PTR-Qi-TOF-MS

Comparison of water vapour mixing ratios and fluxes measured by the IRGA and the PTR-Qi-TOF-MS water clusters (m/z 37.028, m/z 55.039) allows estimating the capability of the instrument to measure water vapour fluxes and thereby giving confidence in VOC measurements. The comparison of the mixing ratios (**Figure S6**) shows that the water cluster mixing ratios were not stably correlated to atmospheric water vapour. Moreover, the water clusters seem to be poor proxies of the atmospheric water vapour pressure over the entire period.



Figure S6. Water vapour mixing ratios as measured from IRGA (ICOS), and the PTR-Qi-TOF-MS either calibrated over the entire period or over rolling 48 h.

On the contrary, the comparison of water vapour fluxes as retrieved with an IRGA and the PTR-Qi-TOF-MS water clusters (**Figure S7**) shows a better agreement indicating that the water vapour cluster fluctuations in the PTR-Qi-TOF-MS are correlated to the atmospheric water vapour fluctuations, and hence suggesting that the offset of the PTR-Qi-TOF-MS water cluster may be fluctuating. We can conclude that the PTR-Qi-TOF-MS should be used with cautious to estimate the water vapour fluxes and can hardly be used to measure the water vapour mixing ratios.



Figure S7. Bottom graph: water vapour flux as measured at ICOS, and the PTRMS either calibrated over the entire period or over rolling 48 h. The slope and intercepts of the rolling calibration are also given in the top graph.

5 Evaluating the capability of the PTR-Qi-TOF-MS to measure CO₂ fluxes and mixing ratios

The CO₂.H⁺ channel (m/z 44.99) may be thought to be used for estimating the CO₂ mixing ratio with PTR-Qi-TOF-MS. However, since CO₂ has a proton affinity much lower than H₂O, CO₂.H⁺ is likely produced out of the drift tube in the electromagnetic lenses, and may not be a good proxy of the atmospheric CO₂. It is therefore interesting to check if it is representative of the ambient CO₂ mixing ratios. **Figure S8** clearly shows that the CO₂.H⁺ signal cannot be representative of the CO₂ flux over the period, since daily CO₂ flux changes from negative to positive values with the canopy senescence while the CO₂.H⁺ flux remains negative all the time. Hence, we can conclude that CO₂.H⁺ should not be used as a CO₂ proxy, unless proven by laboratory calibrations.

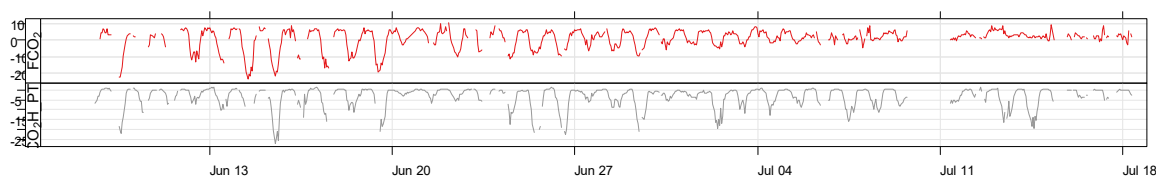


Figure S8. Comparison of the CO₂ flux measured by the IRGA and the CO₂.H⁺ flux measured by the PTRMS.

6 Fragmentations to and from mass m/z 69.070 in relation with E/N

It is well known that some VOC (like MBO, 2-methyl-3-buten-2-ol, $C_5H_{10}O$, m/z 87.080) fragment to m/z 69.07 and that the fragmentation pattern may be dependent on E/N (Zhou et al., 2017; Bachy et al., 2020). It is also known that m/z 69.07 fragment to lighter ions (41.039, 57.070). In this study, E/N changed over the course of the experiment from 150 to 130, giving the opportunity to check its effect on the fragmentation of m/z 69.07 fragments present on m/z 69.07. Karl et al. (2012) showed that isoprene and MBO could be separated by using NO^+ ionisation, which produces the ion m/z 68.062 ($C_5H_8^+$). Since our PTRMS produces also a small quantity of NO^+ , but also O_2^+ , which would lead to the same ionisation of isoprene to m/z 68.062, we tracked m/z 68.062 and found a high correlation between mixing ratios at m/z 68.050 and m/z 69.070 with E/N 150 (spearman correlation 0.97), which was a bit lower with E/N 130 (0.92), suggesting that heavier ions may be fragmenting at m/z 69.070. At E/N = 150, m/z 69.070 was also highly correlated with ions m/z 41.039 (corr. 0.97) and 57.070 (corr. 0.98), as expected. At E/N = 130, the correlations with these ions are lower, suggesting less fragmentation of isoprene to these ions at that E/N state. **Figure S9** shows that m/z 68.062, when scaled up by the slope of the regression between 69.07 and 68.062 obtained for E/N = 150 follows well the m/z 69.07 during the period with E/N=150. When multiplied by the same slope obtained for E/N=130, we have an upper estimation of the m/z 69.070 value at E/N=150. This suggests indeed that almost half of the m/z 69.070 was fragmented for E/N 150.

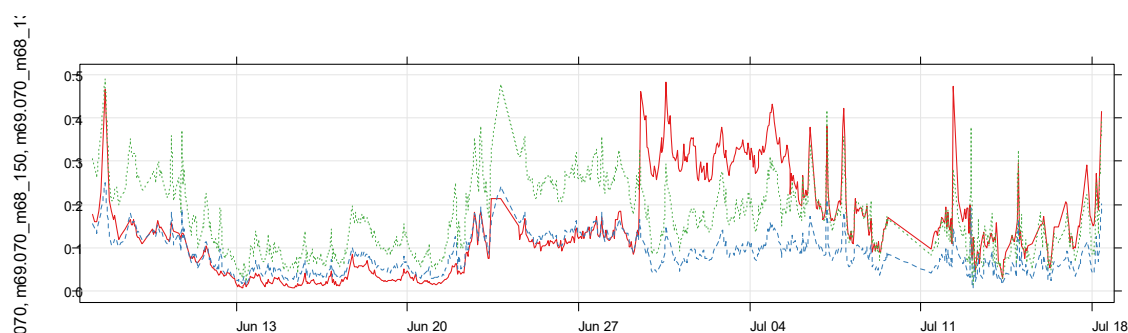


Figure S9. Time course of m/z 69.070 (red) and m/z 68.049*12.3 (grey) mixing ratios (top) and fluxes (bottom) over the course of the experiment. E/N changed from 150 before the 29 June to 130 afterwards

7 Compounds tentative identification

Table S2. VOC tentative identification table

See file *Loubet-COV3ER-wheat-2016-EC-Supp.Mat-VF.docx*

8 Mixing ratio correlation analysis

Correlation between ions mixing ratios was found to be a power tool to identify possible fragments, and resolution issues. Table S2 shows the correlation coefficients over the entire period, and over the period with $E/N = 130$ and 150.

Table S3a. Ions for which 1h-averaged mixing ratio have a Pearson correlation coefficient larger than 0.99 over the entire experiment

File COV3ER_2016_dataset-Correlation-Analysis.0.99.csv

Table S3b. Same as Table S2a with $E/N = 130$ for correlation larger than 0.8

File COV3ER_2016_dataset-Correlation-Analysis.0.9.EN130.xlsx

Table S3c. Same as Table S2a with $E/N = 150$ for correlation larger than 0.9

File COV3ER_2016_dataset-Correlation-Analysis.0.9.EN150.xlsx

9 Wind roses analysis

Figure S10 shows wind roses of methane, NO and N_2O measured at the site. Methane shows the typical wind rose for compounds emitted by the farm, since it is a good tracer of farm emissions. On the opposite, NO is a good tracer of the traffic contribution from the nearby road and the city of Paris on the west. Finally, N_2O shows a quite undetermined wind rose which is expected.

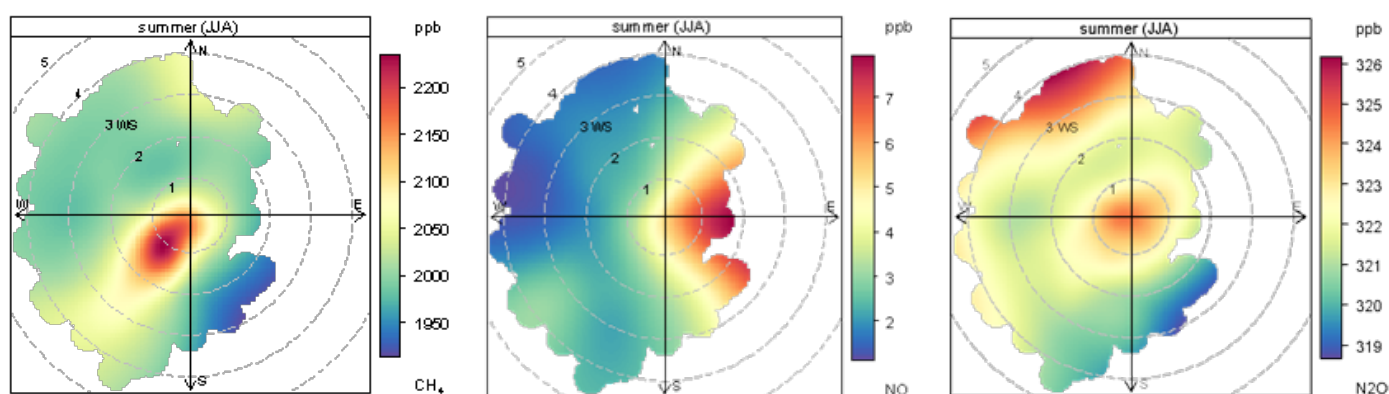


Figure S10. Pollution roses for CH₄, NO and N₂O.

Figure S11 shows the wind roses for all the VOC compounds that were identified as coming from the farm. We clearly see an increase in the normalised mixing ratio from the Farm wind sector (~ 200 deg/N). Some ion peaks belong to the same original ion and were not filtered out for this figure (See **Table S2a for correlations**)

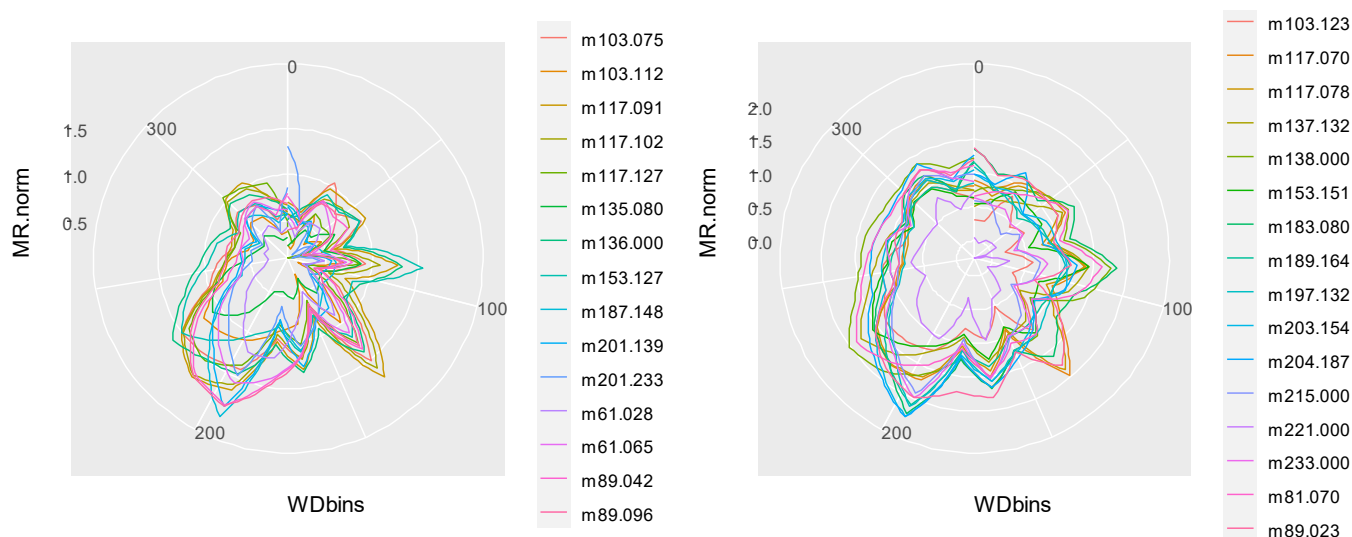


Figure S11. Wind roses of normalised mixing ratios showing an increase when wind is blowing from farm. Normalisation is achieved by dividing the mixing ratio by its standard deviation.

Figure S10 shows the averaged mixing ratio as a function of the average air temperature by separating the farm wind sector and the other wind sectors. We see that for some compounds the difference between Farm sector and the other sector show an optimum temperature around 20°C-25°C, suggesting a biological or chemical optimum process.

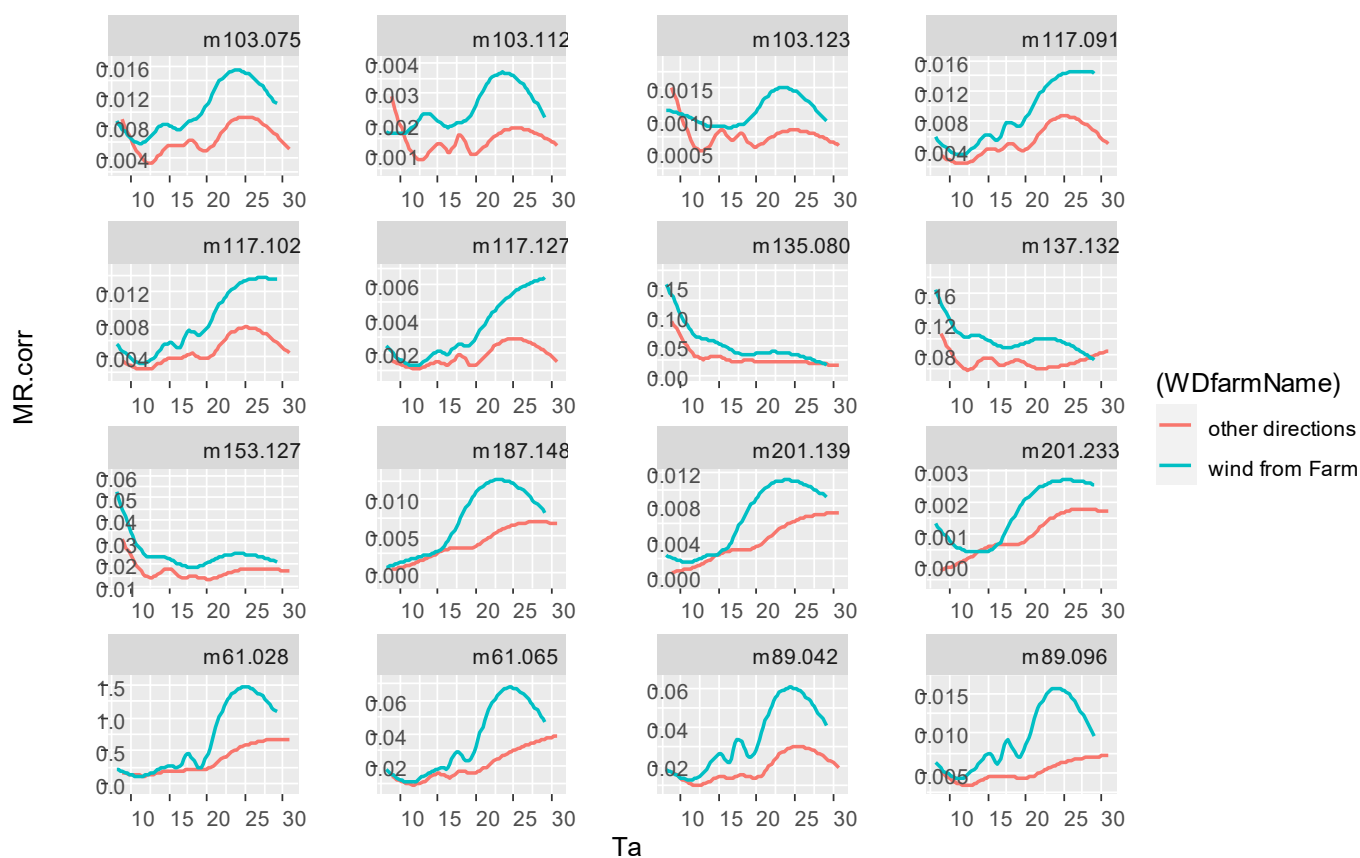
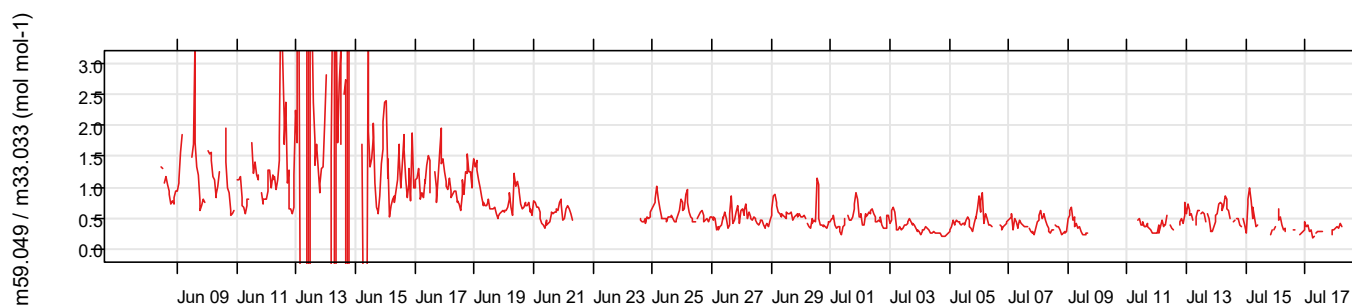


Figure S12. Mixing ratios of compounds identified as coming from the farm, as a function of air temperature.

10 Ratio of acetone to methanol mixing ratios at the site

Acetone to methanol mixing ratios is a quantity measured in many atmospheric chemistry studies. **Figure S13** shows this ratio over the course of the experiment.



260 **Figure S13. Ratio of acetone to methanol mixing ratios at 2.7 m above the ground as a function of time.**

11 Flux limit of detection (LOD)_f.

265 The flux limit of detection was computed following the methodology of Wienhold (1994). **Figure S14** shows LOD_f and averaged fluxes for all ions that matches the condition that the flux is larger than 3 times the overall LOD. The hourly averaged LOD_f is much higher since it does not integrated over the large number of samples collected during the experiment (see computation details in the text).

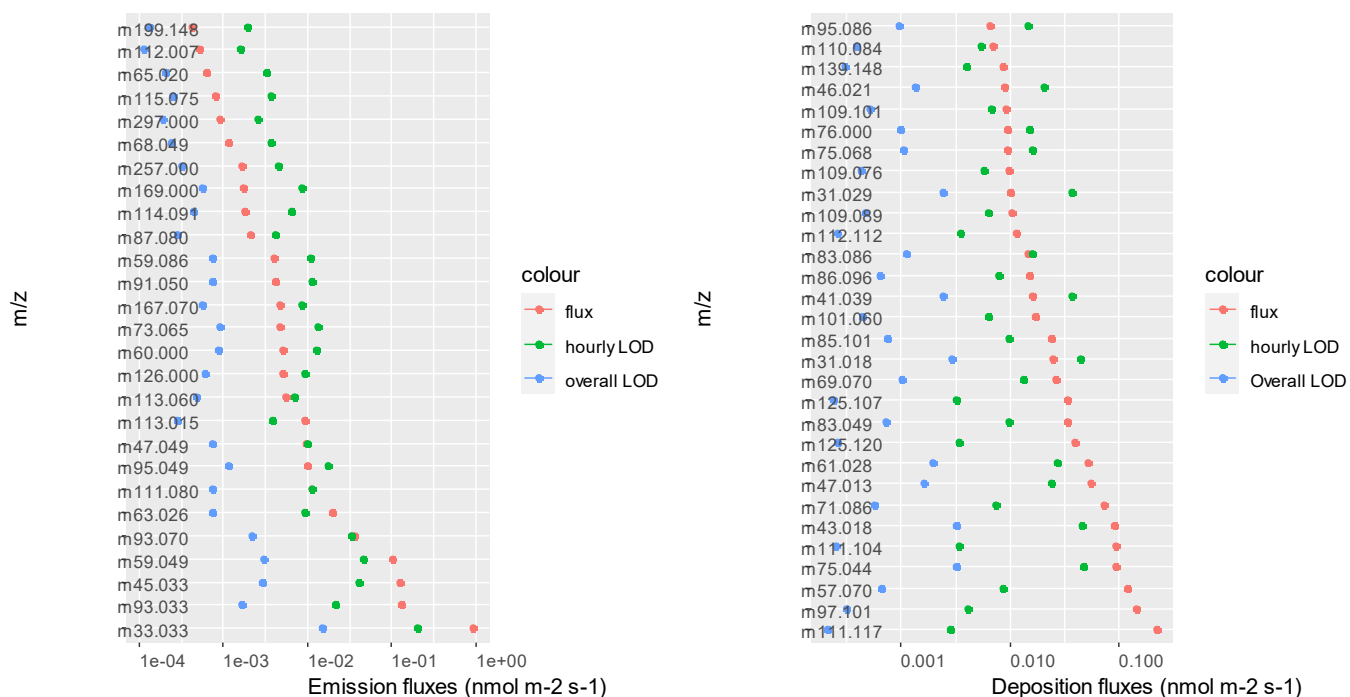


Figure S14. Mean fluxes and LODf of 30 most emitted (left) and most deposited (right) ions over the entire period. Hourly averaged LODf and LODf computed over the whole period are shown.

12 Non-VOC species mixing ratios

12.1 Ozone and nitrogen oxides monitoring

Ozone (O₃), and nitrogen oxides (NO and NO₂) were monitored at the reference height with the same line as the Eddy-Covariance. Air was subsampled through a Teflon pump (KNF 840.FT.18) from a flow rate in excess of 5 L min⁻¹ to the analyser sample flow rates. Tubes were heated to 60°C. A chemiluminescence analyser (42C, ThermoEnvironment, USA) was used for NO and NO₂, and a UV absorption spectrometry analyser (49i, ThermoEnvironment, USA) was used for O₃. The analysers were logged by the same Labview application at 20 Hz and averaged at 5 min. The NO/NO₂ and O₃ analysers were calibrated using a gas phase titration (GPT) unit (SX6000, LNI, SW) with a high quality grade zero air cylinder (99.9999%, Air Liquide, FR) and a 20 ppm NO cylinder (high grade, Air liquide, FR). Zero and 80 ppb of NO were generated for NO calibration. For NO₂ and O₃, a prescribed concentration of O₃ was added in the GPT stream which induced a decrease of NO that corresponded to the amount of O₃ that reacted with NO and was used to calibrate the NO₂ and O₃. The calibration uncertainty was evaluated as 2% for NO_x and 3% for O₃.

12.2 Evolution of the non-VOC mixing ratios over time

The CO₂ mixing ratios varied from 363 to 526 ppm and showed a typical daily pattern for a measurement over a crop with largest values at night when the respiration was large and mixing was low, and lowest values during the day when absorption and mixing were both large (**Figure S15**). The slowing down of the crop photosynthesis was characterised by the increase of the daily minimum CO₂ mixing ratios, while large night-time values

observed towards the end of the campaign rather translate stable atmospheric conditions. During windy nights CO₂ mixing ratio remained low due to good mixing of the boundary layer. Water vapour mixing ratios varied quite a lot from 10 to 25 ppth and showed an increase during 20-25 June following the main precipitation event and were the lowest the 11-14 July. There was no clear daily pattern of water vapour mixing ratios, indicating, as expected, that the daily pattern in RH was mostly related to temperature change (**Figure 4a**).

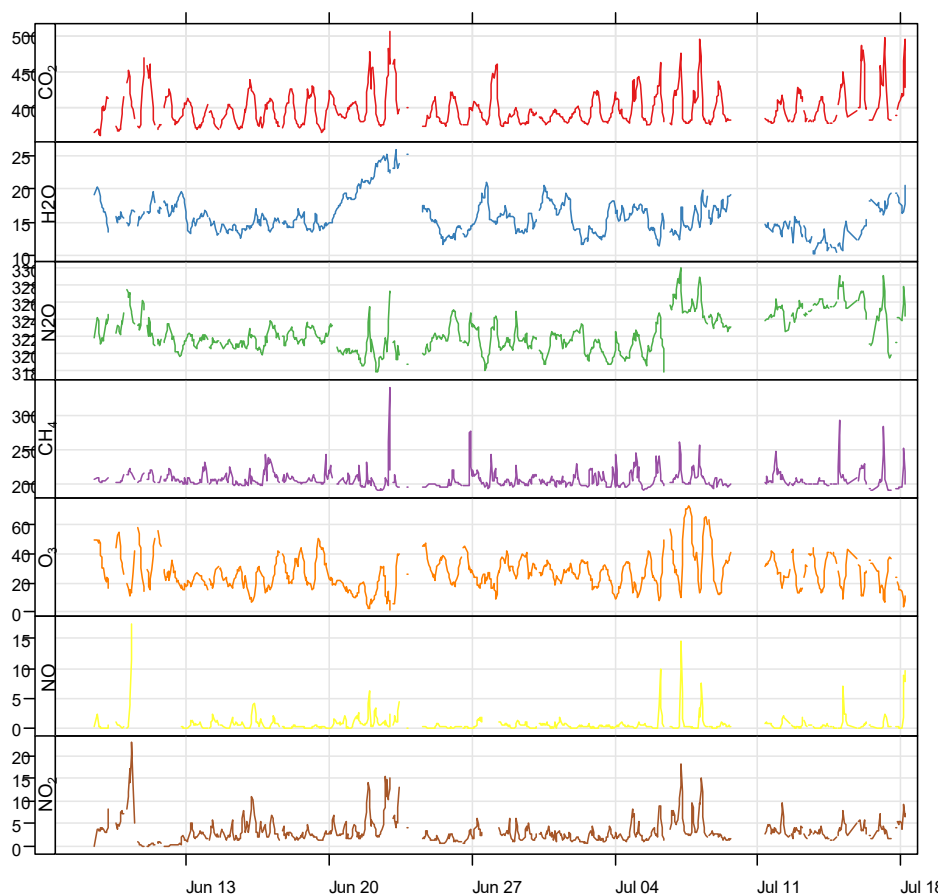


Figure S15. Mixing ratios of CO₂ (ppm) , H₂O (ppth), CH₄ (ppb), O₃ (ppb), NO (ppb) and NO₂ (ppb).

The CH₄ mixing ratio varied from 1907 to 3402 ppb and showed a slight daily pattern similar to CO₂ but with very marked peaks that occur mostly during nights and can be attributed to advection of methane from the nearby dairy farm as clearly showed in **Figure S10**. The ozone mixing ratio varied from 1.5 to 73 ppb and showed a marked daily pattern with daily maximum occurring in the afternoon and night time minimums. The largest concentrations occurred during the warmest periods in early June and July which also corresponded to peaks in NO and NO₂ mixing ratios generated by regional traffic peaks due to the summer holidays rush. NO varied from 0.01 to 17 ppb and peaked at rush hours and during calm nights. An increase was also observed during the slightly rainy period (13-25 June) which may be due to local NO emissions from soils. The NO₂ mixing ratio varied from 0 to 23 ppb and mostly increased in air masses coming from Paris, which also corresponds to the flux footprint being the lowest (east-north-east).

14 Isoprene and Monoterpenes fluxes

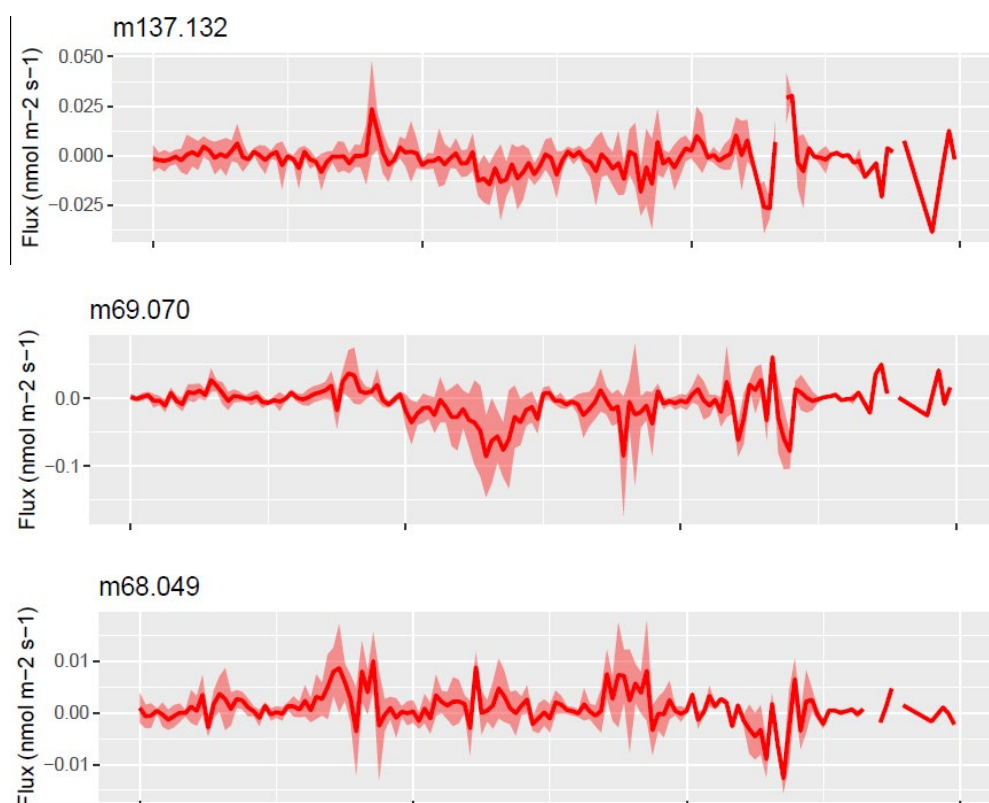


Figure S16. Fluxes of isoprene and monoterpenes over the wheat canopy. The x-axis shows the week number. In each week, the diel cycle is shown with mean and standard deviation.

Supplementary material references

Ammann, c., brunner, a., spirig, c., and neftel, a.: technical note: water vapour concentration and flux measurements with ptr-ms, atmospheric chemistry and physics, 6, 4643-4651, doi 10.5194/acp-6-4643-2006, 2006.

Bachy, a., aubinet, m., amelynck, c., schoon, n., bodson, b., delaplace, p., de ligne, a., digrado, a., du jardin, p., fauconnier, m. L., mozaaffar, a., muller, j. F., and heinesch, b.: dynamics and mechanisms of volatile organic compound exchanges in a winter wheat field, atmos. Environ., 221, 10.1016/j.atmosenv.2019.117105, 2020.

Holzinger, r., acton, w. J. F., blossom, w. J., breitenlechner, m., crilley, l. R., dusanter, s., gonin, m., gros, v., keutsch, f. N., kiendler-scharr, a., kramer, l. J., krechmer, j. E., languille, b., locoge, n., lopez-hilfiker, f., materić, d., moreno, s., nemitz, e., quéléver, l. L. J., sarda esteve, r., sauvage, s., schallhart, s., sommariva, r., tillmann, r., wedel, s., worton, d. R., xu, k., and zaytsev, a.: validity and limitations of simple reaction kinetics to calculate concentrations of organic compounds from ion counts in ptr-ms, atmos. Meas. Tech., 12, 6193-6208, 10.5194/amt-12-6193-2019, 2019.

- Karl, t., hansen, a., cappellin, l., kaser, l., herdlinger-blatt, i., and jud, w.: selective measurements of isoprene and
330 2-methyl-3-buten-2-ol based on no^+ ionization mass spectrometry, *atmospheric chemistry and physics*, 12,
11877-11884, 10.5194/acp-12-11877-2012, 2012.
- Massman, w. J.: the attenuation of concentration fluctuations in turbulent-flow through a tube, *j. Geophys. Res.-
atmos.*, 96, 15269-15273, doi 10.1029/91jd01514, 1991.
- Wienhold, f. G., frahm, h., and harris, g. W.: measurements of n_2o fluxes from fertilized grassland using a fast-
335 response tunable diode-laser spectrometer, *j. Geophys. Res.-atmos.*, 99, 16557-16567, 10.1029/93jd03279, 1994.
- Zhou, p. T., ganzeveld, l., taipale, d., rannik, u., rantala, p., rissanen, m. P., chen, d., and boy, m.: boreal forest
bvoc exchange: emissions versus in-canopy sinks, *atmospheric chemistry and physics*, 17, 14309-14332,
10.5194/acp-17-14309-2017, 2017.